RSC Advances

PAPER

Cite this: *RSC Adv.*, 2021, **11**, 12141

New insight on the simultaneous H_2 and HNO_2 production in concentrated HNO_3 aqueous solutions under alpha radiation†

Raluca M. Musat, *[a] Jean-Luc Roujou,[a] Vincent Dauvois,[a] Muriel Ferry,[a] Carole Marchand[a] and Gérard Baldacchino [b]

Knowledge of hydrogen and nitrous acid yields ($G(H_2)$ and $G(HNO_2)$) from α radiolysis of nitric acid solutions is of critical importance for the technological aspects of reprocessing of spent nuclear fuel (SNF). This study provides critical information on the *G* values for external alpha irradiation of concentrated HNO_3 solutions. An investigation-specifically developed experimental setup allows performing this investigation without encountering issues related to extreme high local doses. *In situ* monitoring of the UV-visible induced absorption in irradiated HNO_3 solutions permitted quantification of HNO_2 production, and mass spectrometry was used to quantify H_2. The influence of the dose rate and HNO_3 concentration was investigated, and the primary yields of these two species were determined. It was found that dose rate increase leads to diminished production of HNO_2 and H_2, while HNO_3 concentration increase leads to increased HNO_2 formation and reduced H_2 production. The values of the primary yields of these two species were determined and compared to the literature reported values. While the determined values show similar trends as those reported, this study provides accurate radiolytic yields for H_2 and HNO_2 that are radioelement-independent compared to the α radiolysis using radioisotope/HNO_3 mixtures and provides the basis for perfecting numerical codes used for simulating the radiolytic processes associated with SNF reprocessing.

Received 28th November 2020
Accepted 5th March 2021

DOI: 10.1039/d0ra10061g

rsc.li/rsc-advances

Introduction

The share of nuclear energy in the context of climate change and of the 2015 Paris agreement[1] is dependent on many factors, the most important one being closing the nuclear fuel cycle, aiming at turning nuclear energy into a virtually zero waste energy source.

The technology surrounding recycling of nuclear fuel has been developed and implemented on a reasonably large scale in several countries. Historically, the main process used for nuclear fuel recycling is the PUREX (Plutonium and Uranium Extraction) process that relies on separation of Pu and U from spent fuel dissolved in HNO_3. The challenge however remains the recovery of all-long lived actinides and recycling them so as to produce short lived fission products, improving the proliferation resistance, reducing waste volume, and making this process cost-effective. For any large-scale separation process to be adopted and fulfil the above requirements, it must be robust under high dose-rate radiation. The effect of radiation on solvent (HNO_3) extractions may result in decreased ligand concentrations, and accumulation of possibly dangerous degradation products. Among these, the most hazardous product is H_2 that can be formed during the radiolytic degradation of HNO_3,[2–4] due to its flammability range, low ignition energy and high deflagration index[5,6] inside a canister. Due to the multi-component aspect of spent nuclear fuel, a multidirectional approach is needed, taking into account the alpha, beta and gamma radiation induced degradation. Many studies were dedicated to the radiolytic degradation of HNO_3 soon after the development of the PUREX process in the '50s, providing a wealth of information on the radiolytic mechanism and yields of H_2, $NO_3^{\bullet}$ and NO_2^-/HNO_2 in the γ[3,7–25] or β radiolysis[8,16,17,22,26–37] of aqueous nitrate and nitric acid solutions. However, fewer studies have been dedicated to the α radiolysis of these solutions, and the majority of these investigations were performed in the radiolysis of HNO_3 in the presence of radionuclides (^{243}Am, ^{241}Am, ^{244}Cm, ^{210}Po, ^{240}Pu, ^{238}Pu).[3,4,38–51] The formation of radiolytic products (H_2, O_2, H_2O_2, $NO_3^{\bullet}$ and NO_2^-/HNO_2) is generally evaluated using direct methods such as spectrophotometry, gas chromatography, ion chromatography or mass spectrometry[40] or indirect methods such as the classical or modified Shinn[52,53] or Ghormley method.[54] For the gas detection, all measurements are performed by sampling the headspace at the end of irradiations or at different residence

[a]*DES – Service d'Étude du Comportement des Radionucleides (SECR), CEA, Université Paris Saclay, F-91191, Gif-sur-Yvette, France. E-mail: rmusat@gmail.com*

[b]*Université Paris-Saclay, CEA, CNRS, LIDYL, F-91191 Gif-sur-Yvette, France*

† Electronic Supplementary Information (ESI) available. See DOI: 10.1039/d0ra10061g

times and replacing the sampled gas by laboratory air. These studies unanimously point to a decrease in the production of H_2, and increased NO_2^-/HNO_2 production with increasing HNO_3 concentration. Elevated linear energy transfer (LET) associated with α irradiation implies generally higher primary yields (*G* values) than those corresponding to β and γ rays, due to increased second order processes as a result of closely spaced spurs and intra-track recombination favouring molecular products yields.[55,56] The measured *G*-values of H_2 range between $9.1 \times 10^{-9} - 4.6 \times 10^{-8}$ mol J^{-1} and 1.93×10^{-7} mol J^{-1} for pure water under γ[55,57,58] and α[57] irradiation respectively, decreasing to 2.1×10^{-9} mol J^{-1} for 6 mol dm^{-3} HNO_3, under γ radiation. The vast majority of these studies has been performed using radionuclides as α sources, raising the problem of nuclides–specific yields and chemical interactions.

In this article we investigate, using energetic external helions, the α-radiation processes occurring in nitric acid solutions with concentrations ranging from 2 to 5 mol dm^{-3}. For gaseous products analysis, we perform sampling of the headspace using volumes that do not disturb the system and/or do not require replacing them with laboratory air that may affect the investigated process. A specially designed quartz cell allowing fast sample circulation and dose evaluation, enables us to perform the *in situ* dosimetry and follow-up experiments. Comparison with the dose evaluated from the α particle flux and from *in situ* Fricke dosimetry shows agreement, ensuring that the extremely high doses generally associated with the use of particle accelerators are eliminated. At the same time, this study does not involve the use of radioelements as α-source, avoiding their chemical implication in the system and supplies independent radiolytic yields. The information provided by these measurements offers a comprehensive understanding of the radiolytic processes occurring in HNO_3, creating a baseline for evaluations of future nuclear solvent extraction systems.

Experimental

HNO_3 70% was purchased from Sigma-Aldrich and used without further purification. The investigated solutions are prepared from its dilution to reach 2, 3, 4 and 5 mol dm^{-3} HNO_3 using ultrapure Milli-Q water with less than 5 ppb organic carbon and a resistivity of 18.2 MΩ cm. 100 ml of fresh solutions are prepared prior to irradiations. The physicochemical properties of the investigated solutions are presented in Table 1.

Table 1 Physicochemical properties of the investigated solutions. f_s, f_w are the electron fractions of the solute and water respectively. P is the density of the solutions, and *F* is the dose factor calculated according to eqn (2)

$[HNO_3]$ (mol dm^3)	ρ (kg cm^{-3})	f_s	f_w	*F* (kg cm^{-3})
0	1.00	0	1	1
2	1.06	0.11	0.89	1.053
3	1.09	0.16	0.84	1.08
4	1.1	0.21	0.79	1.1
5	1.13	0.26	0.74	1.13

For the irradiations, a special monoblock quartz cell was developed that allows continuous circulation of the solution, avoiding accumulation of degradation products and exalted local doses. The total volume of the irradiation cell is 200 ml, and the volume of the irradiated solution is 100 ml, keeping a liquid : gas ratio of 1 : 1. Alpha particles delivered by the cyclotron enter the cell through a quartz window with a thickness of 500 μm, and a surface diameter of 6 mm. The beam diameter is fixed at the same size as the entrance window, so no gas phase irradiation occurs. Using a BVP-Z standard Ismatec pump (IDEX Corp., Cole-Palmer, DE) pump, the solution is continuously flown, at a rate of 3.6 dm^3 min^{-1}, so that the solution passes in a thin jet in front of the quartz window and is then sprayed onto the cell walls, favouring the liquid–gas exchange, and allowing the two phases to reach an equilibrium very efficiently. The irradiated solution is then injected into a 1 cm optical pathlength quartz cell (Hellma Analytics, DE), before returning to the irradiation loop. An optical fiber-connected spectrometer (AvaSpec, Avantes, NL) allows *in situ* monitoring of the UV-vis absorption inside the cells. The spectra are recorded for the entirety of the irradiation (5400 s for each sample), with spectra collected every 60 s as an average of 50 scans, in the wavelength range from 300 to 400 nm. To this irradiation cell, a loop is attached with a gas micro-pump (KNF, DE) that continuously circulates the gaseous phase. Periodically, the gas phase is sampled using a home-built remotely controlled electro-valves system. Each gas sample consists of a 2 ml volume. The gas samples are analysed post-irradiation using a Prisma Pro QMG 220 gas phase quadrupole mass spectrometer (Pfeiffer Vacuum, DE) to quantify the production of H_2. The Prisma Pro QMG 220 has a quadrupole analyser QMA 200 and yttriated iridium filaments, allowing detection in the mass range 1–100 u, with a resolution of 0.5 u, and a minimum detection limit of 3×10^{-15} mbar. The sampled volume does not induce any disturbance in the measurement, as verified by irradiating 2 mol dm^{-3} solutions of HNO_3, at a dose rate of 0.11 Gy s^{-1}. These solutions were irradiated for 7200 s, and for 14 400 s. In the first solution irradiation case the gaseous atmosphere is sampled every 1200 s, whereas for the second irradiated solution, the sampling started 7200 s after the beginning of the irradiation, every 1200 s. The coherence of data and correspondence of hydrogen concentration at 7200 s (832 Gy) – last point of the first solution and first point of the second solution – evidence that no perturbation was induced by sampling the gas atmosphere. Fig. 1S in ESI† presents these data.

All irradiations are performed at the CEMHTI cyclotron (Orleans, France) that delivers α particles with an energy of 45 MeV. The delivered helions pass through titanium screen sheets and the quartz window before entering the solution, losing part of their energy. The energy loss was calculated using SRIM (The Stopping Power and Range of Ions in Matter), based on the TRIM code,[59,60] with an evaluated energy inside the irradiation cell at 12.98 MeV, and the LET of the helions at 102×10^{-3} MeV μm^{-1}.

The flux of particles within the irradiation cell is measured using a Faraday cup, and is set at 1, 2.5, 4, 5 and 10 nA before

experiments. The irradiation time for each sample is of 5400 s. The dose rate is calculated considering the α particle flux and energy according to eqn (1):

$$D = \frac{IE}{2qVF} \quad (1)$$

where I is the current (A), E is the alpha particles energy (J), q is the electron charge (1.6×10^{-19} C), V the irradiated volume (m^3), and F the dose factor (kg m^{-3}) given by:

$$F = \rho \times \frac{p \times \frac{Z_{HNO_3}}{M_{HNO_3}} + (100 - p) \times \frac{Z_{H_2O}}{M_{H_2O}}}{100 \times \frac{Z_{H_2O}}{M_{H_2O}}} \quad (2)$$

Because of the continuous circulation (flow rate = 60 cm^3 s^{-1}) of the target solutions inside the irradiation cell, the locally irradiated volume, V_i ($V_i = S \times l$, S – beam facing cell surface, l – penetration depth of the α particles $l = 163.4$ μm from SRIM calculations) is constantly refreshed, so that in one second the irradiated volume is $V = 60$ cm^3. The evaluated dose rates for the set currents are presented in Table 2.

The maximum dose rate deposited was evaluated by looking at the Bragg curve (presented in Fig. 2S†) in our solution, determined using the SRIM software,[59] according to:

$$D_{max} = \frac{I\left(\frac{dE}{dx}\right)_{max} \times l}{2qVF} \quad (3)$$

where I is the current (A), $\left(\frac{dE}{dx}\right)_{max}$ is the LET at Bragg peak (keV μm^{-1}), l the penetration depth of the α particles (163.4 μm), q is the electron charge (1.6×10^{-19} C), V the irradiated volume (m^3), and F the dose factor (kg m^{-3}). The evaluated maximum dose rates are presented in Table 2.

Prior to all irradiation, an *in situ* dosimetry is also performed using the super Fricke dosimeter, with the UV absorption of the irradiated solutions monitored in real-time using two 10 m optical fibers-coupled AvaSpec – dual channel spectrophotometer (Avantes. NL), attached to the quartz optical cell. The super Fricke dosimeter resides on the classical chemical dosimeter principles: oxidation of Fe^{2+} to Fe^{3+} by the radiolytically produced oxidizing species, but its limited dose range is extended by increasing the O_2 and ferrous sulfate concentrations.[61] Solutions of 10^{-2} mol dm^{-3} $(NH_4)_2Fe(SO_4)_2$ (>99%, AnalaR Normapur, UK) are prepared in 0.4 mol dm^{-3} H_2SO_4 (>98%, Carlo Erba, IT), with 10^{-3} mol dm^{-3} NaCl (Sigma-Aldrich, DE) added to suppress the effect of any impurities and bubbled with O_2 prior to irradiations. The ferric ions' concentration is monitored following the absorption of target solutions at 304 nm ($\varepsilon = 2197$ M^{-1} cm^{-1}). According to the literature, the radiolytic yield of ferric ions for α particles of 12.98 MeV was extrapolated at 6.22×10^{-7} mol J^{-1}.[62–65] From the evolution of the absorbed dose in time, calculated according to eqn (4) and presented in Fig. 3S† in ESI,† we can evaluate the dose rate. The obtained values are presented in Table 2.

$$D_{Fricke} = \frac{[Fe^{3+}]}{G(Fe^{3+})F} \quad (4)$$

For the discussion herein, the dose rate we consider in all yield evaluations is the one measured using the super Fricke system, as it is determined under the same experimental conditions as the measurements in HNO_3 solutions.

Table 2 Dose rates evaluated from the alpha particle flux and from *in situ* Fricke dosimetry for the chosen current intensities

Current (nA)	D (Gy s^{-1})	D_{max} (Gy s^{-1})	D_{Fricke} (Gy s^{-1})
1	0.105	0.31	0.11
2.5	0.26	0.78	0.32
4	0.42	1.25	0.52
5	0.525	1.57	0.65
10	1.05	3.14	1.15

Results and discussion

Nitrous acid (HNO_2) and H_2 are the most important stable radiolytic products issued from exposure of HNO_3 solutions to high ionizing radiation fields, and that can have deleterious effects on the reprocessing technology. HNO_2 can react with actinides, changing their oxidation state, impacting their separation and extraction efficiency, while production and accumulation of H_2 is associated with flammability hazards.

The principal reactions occurring when ionizing radiation passes HNO_3 aqueous solutions are listed in Table 3. Nitrite ions are produced indirectly *via* attack on nitrate ions by the water radiolysis primary species (reactions (13)–(31)) or directly by ionizing radiation (reaction (9)). Kazanjian *et al.*[2] showed that the formation of HNO_2 in HNO_3 in solutions of concentrations higher than 1 mol dm^{-3} is a result of both direct and indirect action of ionizing radiation; Balcerzyk *et al.*[35] showed that even in HNO_3 solutions of concentrations of 1 mol dm^{-3}, the direct effects of ionizing radiation have a non-negligible contribution to the formation of nitrate radicals or ions, which in turn can lead to formation of nitrite. Considering the acidity of the investigated solution and following its pK_a value: $pK_a(HNO_2/NO_2^-) = 3.24$ at 25 °C,[66] nitrite ions exist as nitrous acid.

The time evolution of the transient absorbance spectra recorded up to 5400 s with the AvaSpec fiber-coupled spectrometer is presented in Fig. 1. The 3D plot and time slices of the recorded data show the well-known spectrum of HNO_2 with three absorbance maxima at 348, 358 and 372 nm.[33,67] From Fig. 1, we extracted the time evolution of the absorbance at 358 nm, and converted it into HNO_2 formation ($\varepsilon_{358nm} = 57.05$ M^{-1} cm^{-1};[68]).

While for low concentrations of HNO_3 (<1 mol dm^{-3}), the indirect effects represent the exclusive nitrite formation mechanism, this is not the case for the investigated solutions in this study: even for the lowest concentration investigated, 2 mol dm^{-3} HNO_3 solution, as we can see from the electron fraction of NO_3^- relative to water (Table 1), 11% of the deposited dose is

Table 3 Main reactions occurring in the radiolysis of concentrated nitric acid

$H_2O \rightsquigarrow e^-_{pre}, e^-_{sol}, H_2O^{\bullet+}, H_3O^+, OH^\bullet, H^\bullet$		(5)
$H_2O \rightsquigarrow H_2O^*$		(6)
$H_2O^* \rightarrow H^\bullet + OH^\bullet$		(7)
$H_2O^* \rightarrow H_2 + O^\bullet$		(8)
$NO_3^- \rightsquigarrow NO_3^{-*} \rightarrow NO_2^- + O^\bullet$		(9)
$NO_3^- \rightsquigarrow NO_3^\bullet + e^-$		(10)
$HNO_3 \rightsquigarrow NO_3^\bullet + H^\bullet$		(11)
$HNO_3 \rightsquigarrow HNO_3^* \rightarrow HNO_2 + O^\bullet$		(12)
$O^\bullet(^1D) + H_2O \rightarrow H_2O_2$		(13)
$O^\bullet(^3P) + NO_3^- \rightarrow NO_2^- + O_2$	2.2×10^8;[69]	(14)
$NO_3^- + H^+ \leftrightarrow HNO_3$	$pK_{a15} = 1.4$;[66] ; $k_{15} = 6 \times 10^8$;[32] $k_{-15} = 2 \times 10^{10}$ s^{-1};[32]	(15)
$NO_2^- + H^+ \leftrightarrow HNO_2$	$pK_{a16} = 3.24$; $k_{16} = 5 \times 10^{10}$;[70] $k_{-16} = 3 \times 10^7$ s^{-1};[70]	(16)
$NO_3^- + e^-_{pre} \rightarrow NO_3^{\bullet 2-}$	4.5×10^{12};[71]	(17)
$NO_3^- + e^-_{sol} \rightarrow NO_3^{\bullet 2-}$	9.7×10^9;[72]	(18)
$NO_3^{\bullet 2-} + H_2O \rightarrow NO_2^\bullet + 2OH^-$	1×10^3;[73]	(19)
$NO_3^{\bullet 2-} \overset{H^+}{\Leftrightarrow} HNO_3^{\bullet -}$	$pK_{a20} = 4.8$;[74] 5×10^8;[74]	(20)
$NO_3^{\bullet 2-} + OH^\bullet \rightarrow NO_3^- + OH^-$	2.5×10^9;[73]	(21)
$HNO_3^{\bullet -} \overset{H^+}{\Leftrightarrow} H_2NO_3^\bullet$	$pK_{a22} = 7.5$;[74]	(22)
$H_2NO_3^\bullet \rightarrow NO_2^\bullet + H_2O$	7×10^5;[73]	(23)
$NO_3^- + H^\bullet \rightarrow HNO_3^{\bullet -}$	1×10^7;[73]	(24)
$HNO_3^{\bullet -} \rightarrow NO_2^\bullet + OH^-$	2.31×10^5 s^{-1};[74]	(25)
$H_2O^+ + H_2O \rightarrow OH^\bullet + H_3O^+$	$\sim 10^{13}$;[75,76]	(26)
$H_2O^+ + NO_3^- \rightarrow NO_3^\bullet + H_2O$	1×10^{12};[35]	(27)
$OH^\bullet + HNO_3 \rightarrow NO_3^\bullet + H_2O$	5.3×10^7;[37]	(28)
$OH^\bullet + NO_3^\bullet \rightarrow NO_2^\bullet + HO_2^\bullet$	1.1×10^{10};[36]	(29)
$2NO_2^\bullet \rightleftarrows N_2O_4$	$k_{30} = 4.5 \times 10^8$;[73,77] $k_{-30} = 6.9 \times 10^3$ s^{-1};[77,78]	(30)
$N_2O_4 + H_2O \rightarrow HNO_3 + HNO_2$	18;[77] 1×10^3 s^{-1};[77]	(31)
$NO_2^\bullet + H^\bullet \rightarrow HNO_2$	1×10^{10} s^{-1};[73]	(32)
$H^+ + e^-_{pre} \rightarrow H^\bullet$		(33)
$H^+ + e^-_{sol} \rightarrow H^\bullet$	2.3×10^{10};[79]	(34)
$e^-_{sol} + e^-_{sol} \rightarrow H_2 + OH^- + OH^-$	7.3×10^9;[80]	(35)
$e^-_{sol} + H^\bullet \rightarrow H_2 + OH^-$	2.7×10^{10};[80]	(36)
$e^-_{sol} + OH^\bullet \rightarrow OH^-$	3.5×10^{10};[80]	(37)
$OH^\bullet + HNO_3 \rightarrow NO_3^\bullet + H_2O$	5.3×10^7;[37,81]	(38)
$OH^\bullet + NO_3^\bullet \rightarrow NO_2^\bullet + HO_2^\bullet$	1.1×10^{10};[36]	(39)
$H^\bullet + H^\bullet \rightarrow H_2$	5.1×10^9;[80]	(40)
$H^\bullet + OH^\bullet \rightarrow H_2O$	1.1×10^{10};[80]	(41)
$OH^\bullet + OH^\bullet \rightarrow H_2O_2$	4.8×10^9;[80]	(42)
$H^\bullet + HO_2^\bullet \rightarrow H_2O_2$	1.3×10^{10};[80]	(43)

absorbed by nitrate, leading to the formation of nitrite ions and nitrate radicals (reactions (9) and (10)). The direct action of ionizing radiation can result in the formation of excited $O^\bullet$ atom, in the singlet (^1D) or triplet state (^3P), *via* reaction (9),[69] leading to H_2O_2 (ref. 82–84) or HNO_2 (ref. 69) formation, respectively *via* reactions (13) and (14). When considering the radiolytic yield of HNO_2, we need to also take into account its depletion *via* reactions with species resulting from the radiolysis of water 44–47, or from $NO_3^\bullet$ radicals' consumption of nitrites (reactions (48) and (49)):

$$OH^\bullet + NO_2^\bullet \rightarrow HOONO \quad 4.5 \times 10^9;^{78} \tag{44}$$

$$OH^\bullet + HNO_2 \rightarrow NO_2^\bullet + H_2O \quad 2.6 \times 10^9;^{85} \tag{45}$$

$$H_2O_2 + HNO_2 \rightarrow NO_3^- + H^+ + H_2O$$
$$k_{46} = k'[H^+] = 2.5 \times 10^3\ M^{-1}\ s^{-1} \text{ for } [H^+] = 1 \text{ mol dm}^{-3};^{86} \tag{46}$$

$$H_2O_2 + HNO_2 \rightarrow HOONO + H_2O \quad 1.68 \times 10^{10};^{87}\ 7.2 \times 10^5;^{88} \tag{47}$$

$$NO_3^\bullet + NO_2^\bullet + H_2O \rightarrow 2NO_3^- + 2H^+ \quad 1.7 \times 10^9;^{31} \tag{48}$$

$$NO_3^\bullet + HNO_2 \rightarrow NO_3^- + H^+ + NO_2^\bullet \quad 2 \times 10^8;^{36} \tag{49}$$

Fig. 2 presents the production of HNO_2 in solutions of 2 mol dm^{-3} HNO_3, irradiated at dose rates from 0.11 to 1.14 Gy s^{-1} in the upper panel, and in solutions of several HNO_3 concentrations in the middle panel. As previously observed in α self-radiolysis, the formation of nitrite in HNO_3 is proportional to the absorbed dose. Kazanjian *et al.*[89] observed an increase of nitrite, that reaches a maximum concentration in γ radiolysis for HNO_3 solutions with concentrations lower than 1 mol dm^{-3} while at concentrations higher than 1 mol dm^{-3}, the nitrite increase is linear. The authors suggest that a similar maximum concentration of nitrites for higher doses and β and α radiation,

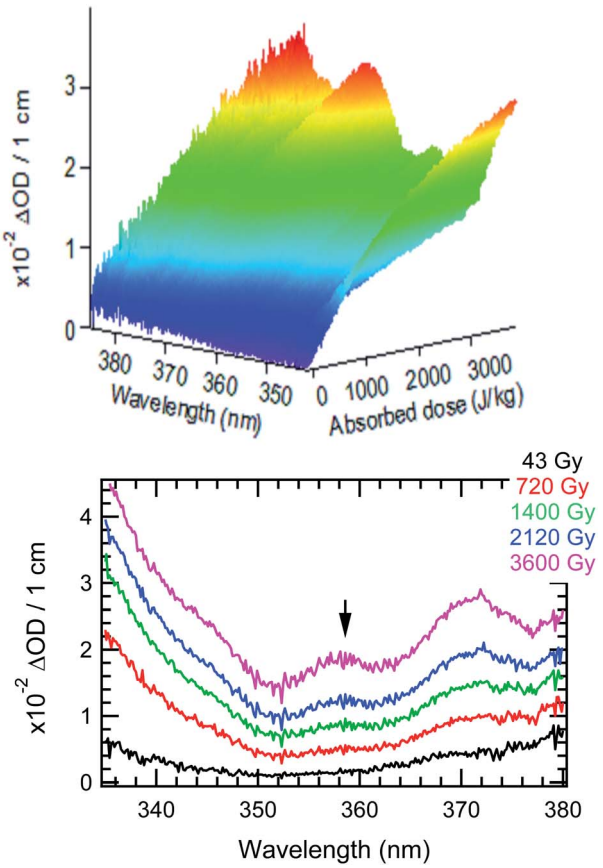

Fig. 1 (Top) Recorded image of the induced absorbance in a solution of 3 mol dm^{-3} HNO_3 by α radiation at a dose rate of 0.64 Gy/s. (Bottom) Same data visualized as transient spectra at different absorbed doses.

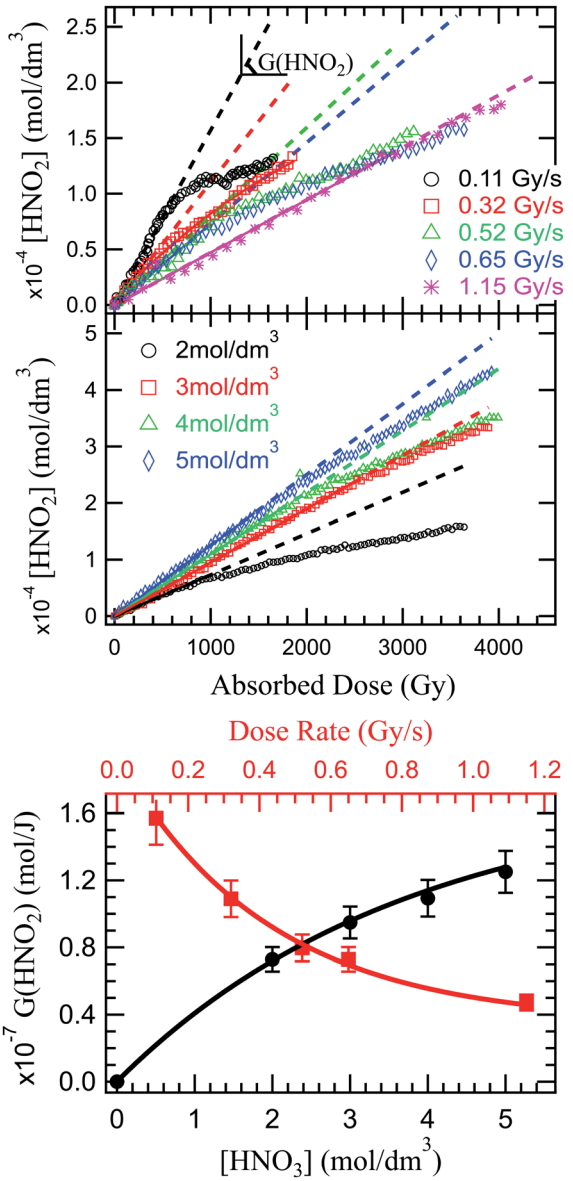

Fig. 2 Top image: dose dependence of the HNO_2 concentration in solutions of 2 mol dm^{-3} HNO_3 under α irradiation at various dose rates. Middle image: HNO_2 concentration as a function of the absorbed dose in solutions of 2, 3, 4 and 5 mol dm^{-3} at 0.64 Gy s^{-1}. Lower image: HNO_2 radiolytic yield dependence on HNO_3 concentration (black) and $G(HNO_2)$ dependence on the dose rate in a 2 mol dm^{-3} HNO_3 solution (red).

is not excluded. Our measurements show that a new regime (break in the slope), or possibly a maximum of the HNO_2 production is reached at the lowest dose rate and lowest concentration. As Fig. 2 shows, such slope-breaking could be expected for the other solutions at higher doses, and for more concentrated HNO_3 solutions at increased dose rates. This new regime of HNO_2 production could correspond to a steady state regime where accumulation of HNO_2 is equilibrated by its degradation and consumption by products resulting from the radiochemical transformations of water (reactions (46)–(49)).

The observed nonlinear dose dependency of HNO_2 concentration is a result of the complex processes involved in its production: both inhomogeneous (intra-track) and homogeneous chemistry are impacting HNO_2 formation.[23] As listed in Table 3, the capture of presolvated and solvated electron by NO_3^- leads to formation of NO_3^{2-}, that can in turn lead to the HNO_2 precursor, $NO_2^{\bullet}$ (reaction (18)), or can be back oxidized by O_2 or H_2O_2 to NO_3^-:

$$NO_3^{\bullet 2-} + O_2 \rightarrow NO_3^- + O_2^{\bullet -} \quad 2.4 \times 10^8; \qquad (50)$$

$$NO_3^{\bullet 2-} + H_2O_2 \rightarrow NO_3^- + OH^{\bullet} + OH^- \quad 1.6 \times 10^8; \qquad (51)$$

H_2O_2 can progressively accumulate in the system, and in time, reactions ((46) and (47)) and (51) start playing a more important role, which may lead to the levelling observed at high doses. Further investigations are required to see if such a stationary regime is also observed for other dose rates and concentrations.

Unlike previous observations that reported no dose rate effect for HNO_2 production in 1 mol dm^{-3} and higher concentrations of HNO_3 at dose rates ranging from 0.93 to 1.5 Gy s^{-1}, but rather assigned observed yield differences as a result of LET effects,[3] a distinct dose rate effect can be observed in the present

investigation: an increase of the dose rate leads to a decrease in $G(HNO_2)$ (Fig. 2 lower panel). An increase in the dose rate will lead to an overlap of the heterogenous zones, and to an increase of biradical reactions, favouring formation of molecular products (H_2O_2 *via* reactions (42) and (43), H_2 *via* (35)–(37)).[90] If the concentrations of HNO_3 solutions is high enough, HNO_3 can interfere in this mechanism. Otherwise, HNO_3 will only react with the molecular products resulting from H_2O radiolysis. Considering the concentration of the studied solutions, the molecular products formed in the radiolysis of HNO_3, can react with the molecular products issued from radiolysis of H_2O. H_2O_2 (H_2 having a low reactivity) is therefore responsible for the decrease in the HNO_2 production, either by consumption of its precursor (reaction (51)) or its decomposition (reaction (46)/(47)). Dose rate also affects the solvated electron yield[91] which in turn is critical in the formation of HNO_2 precursors.

NO_3^- is effectively converted into precursors of $NO_2^\bullet$ (NO_3^{2-}) through capture of presolvated and solvated electrons. Therefore we expect an increase of HNO_3 concentration to lead to an increase of HNO_2 production. Another contribution to this increase could be due to less important destruction of HNO_2 by H_2O_2. Moisy *et al.*[92] showed that in concentrated solutions of HNO_3, the $G(H_2O_2)$ decreases linearly with increasing HNO_3 concentrations. H_2O_2 is mainly formed *via* recombination of $^\bullet OH$ radicals, and increased concentrations of HNO_3 will lead to $^\bullet OH$ scavenging *via* reaction (21) and (28). As the concentration of HNO_3 increases, the dissociation degree decreases, as shown in Fig. 4S (see ESI†). Therefore, the $^\bullet OH$ reaction with the undissociated HNO_3 molecules becomes more important with the increase in HNO_3 concentration, leading to a decrease in H_2O_2, and ultimately to an increase of HNO_2. This is confirmed experimentally in measurement of HNO_2 production in solutions of 2, 3, 4 and 5 mol dm^3 HNO_3 irradiated at the same dose rate (0.64 Gy s^{-1}). The results are presented in Fig. 2 (middle panel).

The radiolytic yields were determined from the slope at origin of these curves, and are presented in Fig. 2 (lower panel). Moisy *et al.*[92] reported that the radiolytic yield rises with the acidity until it reaches a plateau for concentrations of H^+ higher than 1 mol dm^{-3}. However, these measurements were performed in $NaNO_3$–HNO_3 mixtures, and both the NO_3^- concentration and H^+ concentration impact the HNO_2 production. Probably due to the lower NO_3^- concentration, our measurements show no plateau in the investigated HNO_3 concentration range, but we do not exclude its existence at higher concentrations of HNO_3.

In the production of molecular hydrogen in the radiolysis of water, two main mechanisms have been suggested: intra-track chemistry, where the role of the H_2 precursors (reactions (33)–(36)) has been identified and underlined by several authors,[20,50,93] and dissociative chemistry of excited water molecules (reactions (7) and (8)) formed by direct excitation or recombination reaction of the water radical cation with the presolvated electron. In HNO_3 solutions, competition reactions leading to production of H atom through direct effects (reaction (11), and consumption of H_2 precursors (reactions (17) and (18)) occur; but the overall reported trend is a decrease of H_2 in concentrated HNO_3 solutions. As for HNO_2, we looked at what impact of the dose rate and the solution concentration has on H_2 production in the external α radiolysis of HNO_3.

The dose rate effect on the production of solvated electron has been already shown in the literature,[90,91,94] indicating an increased recombination of solvated electron with $H^\bullet$ and $^\bullet OH$ radicals in the complicated process of spur overlap (reactions (36) and (37)). Higher quantities of H_2O_2 produced favorably at higher dose rates and under aerated conditions as is the case of these investigations can also play a role in scavenging this H_2 precursors:[95,96]

$$e^-_{sol} + H_2O_2 \rightarrow OH^\bullet + OH^- + H_2O \quad 1.4 \times 10^{10};^{97} \tag{52}$$

$$e^-_{sol} + O_2 \rightarrow O_2^{-\bullet} \quad 2.3 \times 10^{10};^{97} \tag{53}$$

As the solvated electrons recombinations (reactions (34)–(36)) are a great contributor to H_2 production in the radiolysis of water,[20,98,99] a dose rate increase implying a reduced solvated electron production, will ultimately lead to a decrease in hydrogen production. This behavior is observed experimentally and reported in Fig. 3 (upper panel). The production of H_2 is proportional to the absorbed dose, and inversely proportional to the dose rate. No stationary regime is observed in the production of H_2 under the investigated conditions, leaving room for debate whether this regime exists or not.

It has been shown that the excited water molecule decomposition is the greatest contributor to H_2 formation (~70%) in the radiolysis of water, and the role of the presolvated electron has been underlined.[93] This latter species can undergo dissociative recombination with the parent water cation:

$$e^-_{pre} + H_2O^+ \rightarrow H_2O^* \rightarrow H_2 + O^\bullet \quad 4.3 \times 10^{12};^{93} \tag{54}$$

In HNO_3 solutions, these precursors are scavenged by nitrate ions (reaction (17)). Horne *et al.*[24] showed that these reactions are not sufficient to account for the decrease of H_2 yield in high HNO_3 concentration, and identified the excited water molecule quenching by nitrate ion as responsible for the observed decrease:

$$H_2O^* + NO_3^- \rightarrow NO_3^{-*} + H_2O \quad 1 \times 10^{13};^{24} \tag{55}$$

$H^\bullet$ atoms, which are also produced can at their turn be scavenged by nitrate and nitrite ions and radicals as follows:

$$NO_3^- + H^\bullet \rightarrow HNO_3^- \quad 1.0 \times 10^7;^{78}\ 5.56 \times 10^6;^{100} \tag{56}$$

$$NO_2^- + H^\bullet \rightarrow HNO_2^- \quad 1.61 \times 10^9;^{100} \tag{57}$$

$$HNO_2 + H^\bullet \rightarrow H_2O + NO^\bullet \quad 3.85 \times 10^8;^{100} \tag{58}$$

$$NO_2^\bullet + H^\bullet \rightarrow HNO_2 \quad 1 \times 10^{10};^{101} \tag{59}$$

Previous reports indicated a decreased H_2 production with increased nitrate concentration, due to the scavenging of H_2 precursors (e_{pre}^- and e_{sol}^-) by nitrate (reaction (17) and (18)).

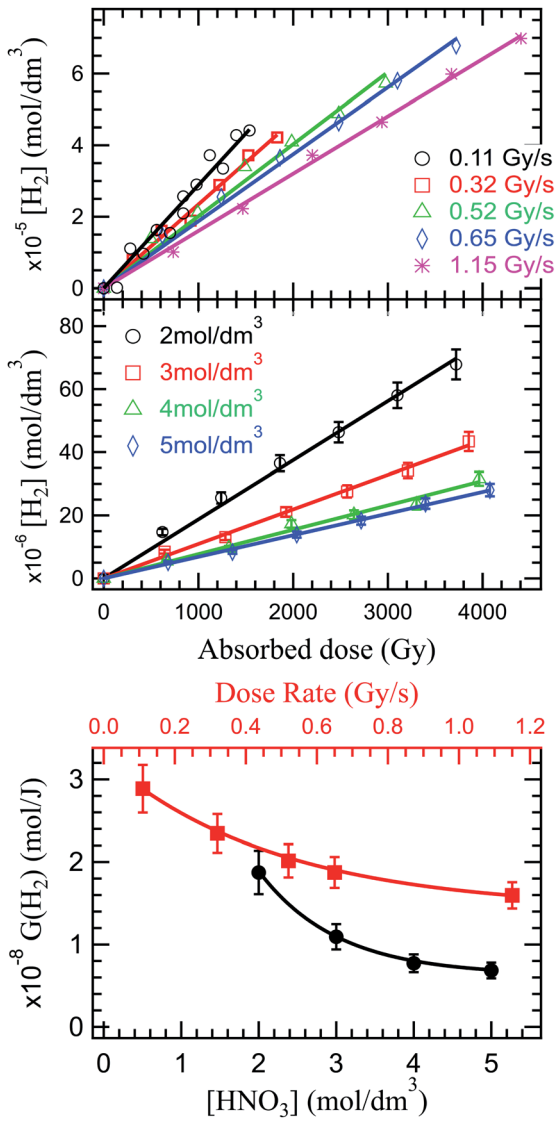

Fig. 3 Top image: dose dependence of the H_2 concentration (top) in solutions of 2 mol dm^{-3} HNO_3 under α irradiation at various dose rates. Middle image: H_2 concentration as a function of the absorbed dose in solutions of HNO_3 for several concentrations indicating a decrease in H_2 with increasing concentrations. Lower image: H_2 radiolytic yield dependence on the concentration of HNO_3 (black) and $G(H_2)$ dependence on the dose rate in a 2 mol dm^{-3} HNO_3 solution (red).

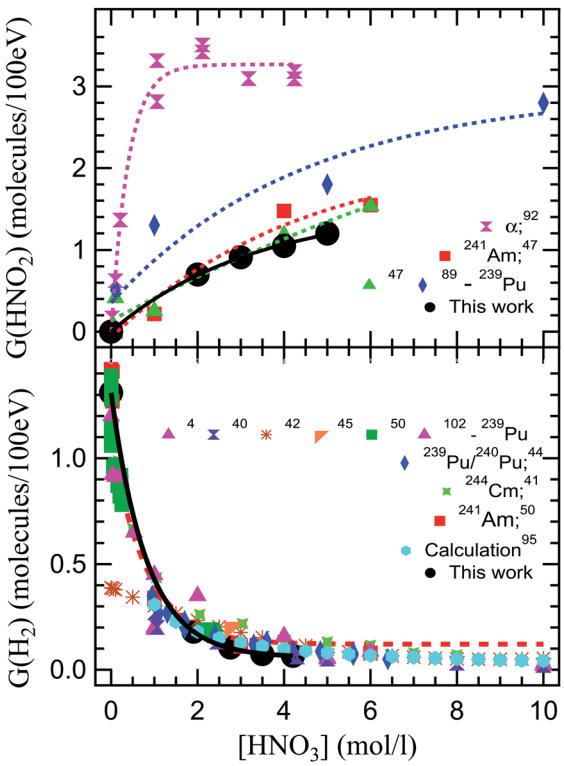

Fig. 4 Comparison of our radiolytic yields of HNO_2 (top image) and H_2 (lower image) with the values reported in the literature. The $G(HNO_2)$ values are extracted from alpha radiolysis of HNO_3 using helions,[92] ^{241}Am,[47] and ^{239}Pu.[47,89] $G(H_2)$ are the values reported in the alpha radiolysis of HNO_3 solutions using ^{239}Pu,[4,40,42,45,50,102] mixtures of $^{239}Pu/^{240}Pu$,[44] ^{244}Cm,[41] ^{241}Am,[50] and calculated values.[51,103]

But, as shown above, a complex series of reactions occurs in HNO_3 solutions that results in a diminished H_2 production decrease. This trend is observed in our investigations in Fig. 3 (middle and lower panel).

Fig. 4 shows a compilation of literature reported values of radiolytic yields of H_2 and HNO_2 measured in the α radiolysis of HNO_3 solutions.

Looking at the previously reported $G(HNO_2)$, our results are closest to the ones obtained for α radiolysis using plutonium nitrate in HNO_3,[47] and rather inconsistent with measurements using helions.[92] However, as mentioned, the external α irradiations were performed in $NaNO_3$–HNO_3 mixtures of constant NO_3^- concentration, by varying the H^+ concentration. These results are obtained from measurements using hydrazinium as an HNO_2 scavenger and following the decay of $N_2H_5^+$ as well as the formation of NH_3. This reaction occurs in competition with H_2O_2 consumption of HNO_2, explaining the observed differences. Pu and Cm self-radiolysis of HNO_3 provide higher values for $G(H_2)$, while Am yielded closer values to these external α investigations. No external α irradiation measurements on the radiolytic yield of H_2 have been reported before this work. Compared to previous reports, we observe that our measurement indicate a slightly lower production of H_2 in the α radiolysis of HNO_3, but careful consideration needs to be taken when such comparisons are made, as the experimental conditions are different. For the α radiolysis investigations, there is a long standing debate over the use of external helions *versus* internal α particle emitters. This concerns the homogenous dose that is usually measured by performing a dosimetry *versus* the very high local dose deposited in solution in the case of external helions, and the localized dose deposition *versus* the calculation of the average deposited doses from the activities of the different actinides used as internal alpha sources. The discrepancies between the local dose deposited by external helions, evaluated from the ion current densities, and the dosimetry evaluated deposited dose have lead authors to the use of radionuclides in the detriment of cyclotrons for α sources. However, this is not applicable for these investigations.

Table 4 H_2 and HNO_2 radiolytic yields as a function of the HNO_3 concentration and as a function of the dose rate in 2 mol dm^{-3} HNO_3

$[HNO_3]$ (mol dm^{-3})	$G(H_2)$ (mol J^{-1})	$G(HNO_2)$ (mol J^{-1})	Dose rate (Gy s^{-1})	$G(H_2)$, 2 mol dm^{-3} HNO_3 (mol J^{-1})	$G(HNO_2)$, 2 mol dm^{-3} HNO_3 (mol J^{-1})
0	1.9×10^{-7};[57]	0	0.11	2.4×10^{-8}	1.6×10^{-7}
2	1.8×10^{-8}	7.2×10^{-8}	0.32	2.3×10^{-8}	1.1×10^{-7}
3	1.1×10^{-8}	9.6×10^{-8}	0.52	2.1×10^{-8}	7.6×10^{-8}
4	7.6×10^{-9}	1.1×10^{-7}	0.65	1.9×10^{-8}	7.2×10^{-8}
5	7.1×10^{-9}	1.3×10^{-7}	1.15	1.7×10^{-8}	4.6×10^{-8}

Continuous intense flow of our solutions insures (see Experimental section – dosimetry) that the irradiated volume is constantly refreshed, avoiding accumulation of degradation products and the mentioned enormous local doses, while insuring the rapid liquid/gas exchange. Moreover, when using internal α particle emitters, radionuclides-specific yields have been recorded due to the progressive disproportionation as a function of the nitric acid concentration induced by the complexing nature of HNO_3 and its chemical involvement in the investigated processes.[46,49,104–113] Simultaneously, investigations using radionuclides may pose exposure and contamination risks to the manipulators and require special equipment for safe handling that render them cumbersome. At the same time, questions are imposed about loss of products during handling. Working in a closed circuit allows us to avoid sampling of the headspace and replacing the sampled volume with laboratory air that can dilute the gaseous volume or induce leaks of H_2 produced, considering the fugacity of H_2 gas. Radioisotope/HNO_3 mixtures result in self-radiolysis and high locally deposited energy, issue partially alleviated by stirring the solutions. Our experimental set-up allowed us to perform experiments, sampling the gas phase without inducing perturbations of the system. To the best of our knowledge, this is the first time that this type of experiment has been performed using external α irradiation.

Conclusions

The two most important species resulting from the radiolysis of HNO_3 are HNO_2 and H_2. When considering the use of HNO_3 in the retreatment of spent nuclear fuel, and therefore its radiolysis due to the high radiation fields it is exposed to, reliable information on the radiolytic yield of $G(HNO_2)$ and $G(H_2)$ is essential. If not scavenged, HNO_2 can be responsible for partitioning failure as it plays on the oxidation state of U, Pu and minor actinides. H_2 concentrations have to be closely monitored in order to avoid its accumulation in the retreatment units and the associated explosion risk. The main scope of these experiments was to gain insight into the α-radiolytic production of these two species, and identify any dose rate and concentration effects. UV-visible spectroscopy and gas mass spectrometry are versatile and extremely sensitive tools for performing quantitative analysis of desired products. Continuously monitoring HNO_2 and H_2 allowed us to perform measurements and quantify their production. These productions show dose rate effects that have been neglected up to now in the production of HNO_2, as well as in the production of H_2. Increasing concentrations of HNO_3 have opposite effects on these products, leading to HNO_2 increase and H_2 decrease.

Table 4 summarizes the determined radiolytic yields as a function of the HNO_3 concentration and dose rate. Our measurements provide accurate values for the radiolytic yields of these species that are chemically independent of any radioisotope that could be used as an α radiation source. The information provided by this study is the first of this kind and starts shedding light on the complexity of the HNO_3 chemical system under irradiation.

From both fundamental and practical aspects, this study paves the way for further investigations on the radiolytic processes occurring in HNO_3 mixtures relevant to SNF retreatment.

Conflicts of interest

There are no conflicts to declare.

Acknowledgements

The authors would like to extend their gratitude to the entire CEMHTI team (Orléans, France. CNRS Campus) without whose help these time consuming and challenging experiments could not have been possible. We address special thanks to Thierry Sauvage and Dominique Baux for their constructive assistance in using the cyclotron installation. The authors acknowledge the financial funding from ORANO, EDF and CEA that made this project happen. The authors would like to thank Virginie Blin, COSTO project (ORANO/EDF/CEA) coordinator for her continuous support.

Notes and references

1 Paris Agreement (Dec. 13, 2015), in *UNFCCC, COP Report No. 21, Addendum, at 21, U.N. Doc. FCCC/CP/2015/10/Add*, 1 (Jan. 29, 2016).

2 F. J. Miner, A. R. Kazanjian, A. K. Brown, P. G. Hagan and J. W. Berry, *Radiation Chemistry of Nitric Acid Solutions*, The Dow Chemical Company, United States, 1969.

3 A. R. Kazanjian, F. J. Miner, A. K. Brown, P. G. Hagan and J. W. Berry, Radiolysis of Nitric Acid Solution: L.E.T. Effects, *Trans. Faraday Soc.*, 1970, **66**, 2192–2198.

4 A. R. Kazanjian and D. R. Horrell, Radiolytically Generated Gases in Plutonium–Nitric Acid Solutions, *Radiation Effects: Incorporating Plasma Science and Plasma Technology*, 1972, **13**, 277–280.

5 D. A. Crowl and Y.-D. Jo, The hazards and risks of hydrogen, *J. Loss Prev. Process Ind.*, 2007, **20**, 158–164.

6 F. L. Dryer, M. Chaos, Z. Zhao, J. N. Stein, J. Y. Alpert and C. J. Homer, Spontaneous Ignition of Pressurized Releases of Hydrogen and Natural Gas into Air, *Combust. Sci. Technol.*, 2007, **179**, 663–694.

7 H. A. Mahlman, Activity Concept in Radiation Chemistry, *J. Chem. Phys.*, 1959, **31**, 993–995.

8 L. L. Burger and M. D. Money, *Nitrous Acid Behavior in Purex Systems*, Hanford Laboratories Operation, United States, 1959.

9 H. A. Mahlman, Hydrogen Formation in the Radiation Chemistry of Water, *J. Chem. Phys.*, 1960, **32**, 601–603.

10 H. A. Mahlman, The OH Yield in the Co60 γ Radiolysis of HNO_3, *J. Chem. Phys.*, 1961, **35**, 936–939.

11 H. A. Mahlman, The "Direct Effect" in the Radiolysis of Aqueous Sodium Nitrate Solutions, *J. Phys. Chem.*, 1963, **67**, 1466–1469.

12 M. L. Hyder, The Radiolysis of Aqueous Nitrate Solutions, *J. Phys. Chem.*, 1965, **69**, 1858–1865.

13 M. Daniels and E. E. Wigg, Radiation Chemistry of the Aqueous Nitrate System. I. γ-Radiolysis of Dilute Solutions, *J. Phys. Chem.*, 1967, **71**, 1024–1033.

14 M. Daniels and E. E. Wigg, Radiation Chemistry of the Aqueous Nitrate System. II. Scavenging and pH Effects in the Cobalt-60 Gamma Radiolysis of Concentrated Sodium Nitrate Solutions, *J. Phys. Chem.*, 1969, **73**, 3703–3709.

15 Z. D. Draganic and I. G. Draganic, Studies on the Formation of Primary Yields of Hydrogen Peroxide and Molecular Hydrogen (GH_2O_2 and GH_2) in the Radiolysis of Neutral Aqueous Solutions, *J. Phys. Chem.*, 1971, **75**, 3950–3957.

16 R. W. Matthews, H. A. Mahlman and T. J. Sworski, Elementary Processes in the Radiolysis of Aqueous Nitric Acid Solutions. Determination of Both GOH and GNO3, *J. Phys. Chem.*, 1972, **76**, 2680–2684.

17 P. K. Bhattacharyya and R. D. Saini, Radiolytic Yields $G(HNO_2)$ and $G(H_2O_2)$ in the Aqueous Nitric Acid System, *Int. J. Radiat. Phys. Chem.*, 1973, **5**, 91–99.

18 L. G. Rodenas, R. F. Prini and S. J. Liberman, Radiolysis of Aqueous Solutions of Gadolinium Nitrate, *J. Radioanal. Nucl. Chem.*, 1990, **139**, 277–286.

19 N. Nakagiri and T. Miyata, Evaluation of Value for Hydrogen Release from High-level Liquid Waste, (I). Gamma-Ray Radiolysis of Aqueous Nitric Acid Solutions., *J. At. Energy Soc. Jpn.*, 1994, **36**, 744–751.

20 B. Pastina, J. A. LaVerne and S. M. Pimblott, Dependence of Molecular Hydrogen Formation in Water on Scavengers of the Precursor to the Hydrated Electron, *J. Phys. Chem. A*, 1999, **103**, 5841–5846.

21 K. Yoshida, H. Abe, Y. Yamane, S. Tashiro and K. Muramatsu, *Research on the State-of-the-art of Accident Consequence Analysis Method for Non-reactor Nuclear Facilities*, Japan Atomic Energy Agency, Japan, 2007.

22 G. Elias, PhD thesis, University of Idaho, 2010.

23 G. P. Horne, T. A. Donoclift, H. E. Sims, R. M. Orr and S. M. Pimblott, Multi-Scale Modeling of the Gamma Radiolysis of Nitrate Solutions, *J. Phys. Chem. B*, 2016, **120**, 11781–11789.

24 G. P. Horne, S. M. Pimblott and J. A. LaVerne, Inhibition of Radiolytic Molecular Hydrogen Formation by Quenching of Excited State Water, *J. Phys. Chem. B*, 2017, **121**, 5385–5390.

25 D. Watanabe, Y. Wada, A. Sasahira, M. Itori and T. Ebina, Nitrous Acid Generation From Radiolysis of Nitric Acid Aqueous Solution Under Gas Flow Condition, *J. Nucl. Sci. Technol.*, 2017, **54**, 182–187.

26 R. K. Broszkiewicz, The Radiation-Induced Formation of NO_3 in Aqueous Solutions, *Int. J. Appl. Radiat. Isot.*, 1966, **18**, 25–32.

27 M. Daniels, Radiation Chemistry of the Aqueous Nitrate System. III. Pulse Electron Radiolysis of Concentrated Sodium Nitrate Solutions, *J. Phys. Chem.*, 1969, **73**, 3710–3717.

28 E. Kozłowska-Milner and R. K. Broszkiewicz, Pulse Radiolysis of HNO_3 and HNO_3(aq), *Radiat. Phys. Chem.*, 1977, **1978**(11), 253–260.

29 M. V. Vladimirova, I. A. Kulikov, O. A. Sosnovskii and A. A. Ryabova, Reduction of PuO^{22+} in y Radioysis in Aqueous HNO_3, *At. Energ.*, 1981, **51**, 55–57.

30 P. Neta and R. E. Huie, Rate constants for reactions of nitrogen oxide (NO_3) radicals in aqueous solutions, *J. Phys. Chem.*, 1986, **90**, 4644–4648.

31 Y. Katsumura, P. Y. Jiang, R. Nagaishi, T. Oishi, K. Ishigure and Y. Yoshida, Pulse Radiolysis Study of Aqueous Nitric Acid Solutions: Formation Mechanism, Yield, and Reactivity of NO_3 Radical, *J. Phys. Chem.*, 1991, **95**, 4435–4439.

32 G. A. Poskrebyshev, P. Neta and R. E. Huie, Equilibrium constant of the reaction $^{\bullet}OH + HNO_3 \leftrightarrows H_2O + NO_3$. in aqueous solution, *J. Geophys. Res.: Atmos.*, 2001, **106**, 4995–5004.

33 M. Precek, A. Paulenova, P. Tkac and N. Knapp, Effect of Gamma Irradiation on the Oxidation State of Neptunium in Nitric Acid in the Presence of Selected Scavengers, *Sep. Sci. Technol.*, 2010, **45**, 1699–1705.

34 M. Precek, A. Paulenova and B. J. Mincher, Reduction of Np(VI) in Irradiated Solutions of Nitric Acid, *Procedia Chem.*, 2012, **7**, 51–58.

35 A. Balcerzyk, A. K. El Omar, U. Schmidhammer, P. Pernot and M. Mostafavi, Picosecond Pulse Radiolysis Study of Highly Concentrated Nitric Acid Solutions: Formation Mechanism of $NO_3^{\bullet}$ Radical, *J. Phys. Chem. A*, 2012, **116**, 7302–7307.

36 G. Garaix, G. P. Horne, L. Venault, P. Moisy, S. M. Pimblott, J. Marignier and M. Mostafavi, Decay Mechanism of $NO_3^{\bullet}$ Radical in Highly Concentrated Nitrate and Nitric Acidic Solutions in the Absence and Presence of Hydrazine, *J. Phys. Chem. B*, 2016, **120**, 5008–5014.

37 R. Musat, S. A. Denisov, J.-L. Marignier and M. Mostafavi, Decoding the Three-Pronged Mechanism of $NO_3^{\bullet}$ Radical Formation in HNO_3 Solutions at 22 and 80 °C Using

Picosecond Pulse Radiolysis, *J. Phys. Chem. B*, 2018, **122**, 2121–2129.
38 M. Lefort, Radiochimie des solutions aqueuses: Remarques particulières à l'action des rayons α, *J. Chim. Phys.*, 1954, **51**, 351–353.
39 M. V. Vladimirova, Alpha Radiolysis of Aqueous Solutions, *Russ. Chem. Rev.*, 1964, **33**, 212–220.
40 J. C. Sheppard, *Alpha Radiolysis of Plutonium (IV): Nitric Acid Solutions*, Battelle-Northwest, Richland, Washington Pacific Northwest Lab, United States, 1968.
41 N. E. Bibler, Curium-244 alpha Radiolysis of Nitric Acid. Oxygen Production from Direct Radiolysis of Nitrate Ions, *J. Phys. Chem.*, 1974, **78**, 211–215.
42 A. Maimoni, *Density and Radiolytic Decomposition of Plutonium Nitrate Solutions*, Lawrence Livermore Laboratory, United States, 1979.
43 S. Tachimori, Numerical Simulation for Chemical Reactions of Actinide Elements in Aqueous Nitric Acid Solution, *J. Nucl. Sci. Technol.*, 1991, **28**, 218–227.
44 Y. Kuno, T. Hina and J. Masui, Radiolytically Generated Hydrogen and Oxygen from Plutonium Nitrate Solutions, *J. Nucl. Sci. Technol.*, 1993, **30**, 919–925.
45 J. R. Smith, *Radiolysis Gases from Nitric Acid Solutions Containing HSA and HAN (U)*, Westinghouse Savannah River Company, 1994.
46 M. V. Vladimirova and A. V. Khaperskaya, Mechanism and Kinetics of Rh(IV) Radiation-Chemical Reduction in HNO3 Solutions, *Radiochemistry*, 2003, **45**, 33–39.
47 G. P. Horne, C. R. Gregson, H. E. Sims, R. M. Orr, R. J. Taylor and S. M. Pimblott, Plutonium and Americium Alpha Radiolysis of Nitric Acid Solutions, *J. Phys. Chem. B*, 2017, **121**, 883–889.
48 Z. Liu, Z. Fang, L. Wang, H. He and M.-Z. Lin, Alpha Radiolysis of Nitric Acid Aqueous Solution Irradiated by 238Pu Source, *Nucl. Sci. Tech.*, 2017, **28**, 54.
49 T. S. Grimes, G. P. Horne, C. J. Dares, S. M. Pimblott, S. P. Mezyk and B. J. Mincher, Kinetics of the Autoreduction of Hexavalent Americium in Aqueous Nitric Acid, *Inorg. Chem.*, 2017, **56**, 8295–8301.
50 C. R. Gregson, G. P. Horne, R. M. Orr, S. M. Pimblott, H. E. Sims, R. J. Taylor and K. J. Webb, Molecular Hydrogen Yields from the α-Self-Radiolysis of Nitric Acid Solutions Containing Plutonium or Americium, *J. Phys. Chem. B*, 2018, **122**, 2627–2634.
51 R. Nagaishi, A Model for Radiolysis of Nitric Acid and its Application to the Radiation Chemistry of Uranium Ion in Nitric Acid Medium, *Radiat. Phys. Chem.*, 2001, **60**, 369–375.
52 M. B. Shinn, Colorimetric Method for Determination of Nitrate, *Ind. Eng. Chem., Anal. Ed.*, 1941, **13**(1), 33–35.
53 K. Bendschneider and R. J. Robinson, *New Spectrophotometric Method for the Determination of Nitrite in Sea Water*, University of Washington Oceanographic Laboratories, Seattle, WA, USA, 1952.
54 A. O. Allen, C. J. Hochanadel, J. A. Ghormley and T. W. Davis, Decomposition of Water and Aqueous Solutions under Mixed Fast Neutron and γ-Radiation, *J. Phys. Chem.*, 1952, **56**, 575–586.
55 J. W. T. Spinks and R. J. Woods, *An introduction to radiation chemistry*, Wiley, New York, 3rd edn, 1990.
56 F. Crumière, J. Vandenborre, R. Essehli, G. Blain, J. Barbet and M. Fattahi, LET effects on the hydrogen production induced by the radiolysis of pure water, *Radiat. Phys. Chem.*, 2013, **82**, 74–79.
57 R. Essehli, F. Crumière, G. Blain, J. Vandenborre, F. Pottier, B. Grambow, M. Fattahi and M. Mostafavi, H_2 Production by γ and He Ions Water Radiolysis, Effect of Presence TiO_2 Nanoparticles, *Int. J. Hydrogen Energy*, 2011, **36**, 14342–14348.
58 J. A. LaVerne and L. Tandon, H_2 Production in the Radiolysis of Water on CeO_2 and ZrO_2, *J. Phys. Chem. B*, 2002, **106**, 380–386.
59 J. F. Ziegler and J. P. Biersack, in *Treatise on Heavy-Ion Science: Volume 6: Astrophysics, Chemistry, and Condensed Matter*, Springer US, Boston, MA, 1985, pp. 93–129.
60 J. F. Ziegler, M. D. Ziegler and J. P. Biersack, SRIM – The stopping and range of ions in matter, *Nucl. Instrum. Methods Phys. Res., Sect. B*, 2010, **2010**(268), 1818–1823.
61 R. W. Matthews, Aqueous Chemical Dosimetry, *Int. J. Appl. Radiat. Isot.*, 1982, **33**, 1159–1170.
62 R. D. Saini and P. K. Bhattacharyya, Radiolytic Oxidation of U(IV) Sulphate in Aqueous Solution by Alpha Particles from Cyclotron, *Int. J. Radiat. Appl. Instrum. C Radiat. Phys. Chem.*, 1987, **29**, 375–379.
63 J. A. LaVerne and R. H. Schuler, Radiation Chemical Studies with Heavy Ions: Oxidation of Ferrous Ion in the Fricke Dosimeter, *J. Phys. Chem.*, 1987, **91**, 5770–5776.
64 M. Matsui, H. Seki, T. Karasawa and M. Imamura, Radiation Chemical Studies with Cyclotron Beams, (I): Fricke Solution, *J. Nucl. Sci. Technol.*, 1970, **7**, 97–104.
65 C. Costa, J. Vandenborre, F. Crumière, G. Blain, R. Essehli and M. Fattahi, Chemical Dosimetry during Alpha Irradiation: A Specific System for UV-vis *in situ* Measurement, *Am. J. Anal. Chem.*, 2012, **03**, 6–11.
66 R. M. Smith and A. E. Martell, *Critical Stability Constants: Inorganic Complexes*, Springer-Verlag New York, 1976.
67 J. Chlistunoff, K. J. Ziegler, L. Lasdon and K. P. Johnston, Nitric/Nitrous Acid Equilibria in Supercritical Water, *J. Phys. Chem. A*, 1999, **103**, 1678–1688.
68 E. Riordan, N. Minogue, D. Healy, P. O'Driscol and J. R. Sodeau, Spectroscopic and Optimization Modeling Study of Nitrous Acid in Aqueous Solution, *J. Phys. Chem. A*, 2005, **109**, 779–786.
69 P.-Y. Jiang, R. Nagaishi, T. Yotsuyanagi, Y. Katsumura and K. Ishigure, γ-Radiolysis study of concentrated nitric acid solutions, *J. Chem. Soc., Faraday Trans.*, 1994, **90**, 93–95.
70 Z. B. Alfassi, *N-Centered Radicals*, Wiley, Chichester , New York, 1998.
71 S. M. Pimblott and J. A. LaVerne, On the Radiation Chemical Kinetics of the Precursor to the Hydrated Electron, *J. Phys. Chem. A*, 1998, **102**, 2967–2975.
72 G. V. Buxton, C. L. Greenstock, W. P. Helman and A. B. Ross, Critical Review of Rate Constants for Reactions of Hydrated Electrons, Hydrogen Atoms and Hydroxyl

Radicals ($^{\bullet}OH/^{\bullet}O^{-}$) in Aqueous Solution, *J. Phys. Chem. Ref. Data*, 1988, **17**, 2.

73 T. Loegager and K. Sehested, Formation and Decay of Peroxynitrous Acid: a Pulse Radiolysis Study, *J. Phys. Chem.*, 1993, **97**, 6664–6669.

74 M. Grätzel, A. Henglein and S. Taniguchi, Pulsradiolytische Beobachtungen über die Reduktion des NO_3^- -Ions und über Bildung und Zerfall der persalpetrigen Säure in wäßriger Lösung, *Berichte der Bunsengesellschaft für physikalische Chemie*, 1970, **74**, 292–298.

75 A. Furuhama, M. Dupuis and K. Hirao, Reactions associated with ionization in water: A direct *ab initio* dynamics study of ionization in $(H_2O)_{17}$, *J. Chem. Phys.*, 2006, **124**, 3–13.

76 O. Marsalek, C. G. Elles, P. A. Pieniazek, E. Pluhařová, J. VandeVondele, S. E. Bradforth and P. Jungwirth, Chasing charge localization and chemical reactivity following photoionization in liquid water, *J. Chem. Phys.*, 2011, **135**, 224510.

77 M. Grätzel, A. Henglein, J. Lilie and G. Beck, Pulsradiolytische Untersuchung einiger Elementarprozesse der Oxydation und Reduktion des Nitritions, *Berichte der Bunsengesellschaft für physikalische Chemie*, 1969, **73**, 646–653.

78 T. Loegager and K. Sehested, Formation and Decay of Peroxynitric Acid: A Pulse Radiolysis Study, *J. Phys. Chem.*, 1993, **97**, 10047–10052.

79 C. D. Jonah, J. R. Miller and M. S. Matheson, The reaction of hydrated electron + oxonium. Concentration effects of acid or salts, *J. Phys. Chem.*, 1977, **81**, 931–934.

80 A. J. Elliott and D. M. Bartels, *The Reaction Set, Rate Constants and g-Values for the Simulation of the Radiolysis of Light Water over the Range 20° to 350 °C Based on Information Available in 2008*, Atomic Energy of Canada Limited, Canada, 2009.

81 P. Y. Jiang, Y. Katsumura, K. Ishigure and Y. Yoshida, Reduction Potential of the Nitrate Radical in Aqueous Solution, *Inorg. Chem.*, 1992, **31**, 5135–5136.

82 H. Taube, Photochemical Reactions of Ozone in Solution, *Trans. Faraday Soc.*, 1957, **53**, 656.

83 P. G. Sennikov, S. K. Ignatov and O. Schrems, Complexes and Clusters of Water Relevant to Atmospheric Chemistry: H_2O Complexes with Oxidants, *ChemPhysChem*, 2005, **6**, 392–412.

84 S. Xu, V. Jirasek and P. Lukes, Molecular Dynamics Simulations of Singlet Oxygen Atoms Reactions with Water Leading to Hydrogen Peroxide, *J. Phys. D: Appl. Phys.*, 2020, **53**, 275204.

85 M. Fischer and P. Warneck, Photodecomposition of Nitrite and Undissociated Nitrous Acid in Aqueous Solution, *J. Phys. Chem.*, 1996, **100**, 18749–18756.

86 S. I. Nikitenko, P. Moisy, L. Venault and C. Madic, Kinetics of Nitrous Acid Formation in a Two-Phase Tri-*n*-Butylphosphate–Diluent/Aqueous Nitric Acid Extraction System Under the Effect of Power Ultrasound, *Ultrason. Sonochem.*, 2000, **7**, 135–144.

87 D. Vione, V. Maurino, C. Minero, D. Borghesi, M. Lucchiari and E. Pelizzetti, New Processes in the Environmental Chemistry of Nitrite. 2. The Role of Hydrogen Peroxide, *Environ. Sci. Technol. Libr.*, 2003, **37**, 4635–4641.

88 B. J. Mincher, M. Precek, S. P. Mezyk, G. Elias, L. R. Martin and A. Paulenova, The Redox Chemistry of Neptunium in γ-Irradiated Aqueous Nitric Acid, *Radiochim. Acta*, 2013, **101**, 259–266.

89 F. J. Miner, A. R. Kazanjian, A. K. Brown, P. G. Hagan and J. W. Berry, *Radiation Chemistry of Nitric Acid Solutions*, The Dow Chemical Company, United States, 1969.

90 C. Ferradini and J.-P. Jay-Gerin, La radiolyse de l'eau et des solutions aqueuses : historique et actualité, *Can. J. Chem.*, 1999, **77**, 1542–1575.

91 J. E. Fanning, C. N. Trumbore, P. G. Barkley, D. R. Short and J. H. Olson, Preliminary Report of a Spur Model Including Spur Overlap, *J. Phys. Chem.*, 1977, **81**, 1026–1029.

92 G. Garaix, L. Venault, A. Costagliola, J. Maurin, M. Guigue, R. Omnee, G. Blain, J. Vandenborre, M. Fattahi, N. Vigier and P. Moisy, Alpha Radiolysis of Nitric Acid and Sodium Nitrate with $4He^{2+}$ Beam of 13.5 MeV Energy, *Radiat. Phys. Chem.*, 2015, **106**, 394–403.

93 J. A. LaVerne and S. M. Pimblott, New Mechanism for H_2 Formation in Water, *J. Phys. Chem. A*, 2000, **104**, 9820–9822.

94 C. N. Trumbore, D. R. Short, J. E. Fanning and J. H. Olson, Effects of Pulse Dose on Hydrated Electron Decay Kinetics in the Pulse Radiolysis of Water. A Computer Modeling Study, *J. Phys. Chem.*, 1978, **82**, 2762–2767.

95 A. Mozumder, *Fundamentals of radiation chemistry*, Academic Press, San Diego, 1999.

96 B. J. Mincher, G. Elias, L. R. Martin and S. P. Mezyk, Radiation Chemistry and the Nuclear Fuel Cycle, *J. Radioanal. Nucl. Chem.*, 2009, **282**, 645–649.

97 A. J. Elliot and D. M. Bartels, *The Reaction Set, Rate Constants and g-Values for the Simulation of the Radiolysis of Light Water over the Range 20° to 350°C Based on Information Available in 2008*, Atomic Energy of Canada Limited, Canada, 2009.

98 E. Peled and G. Czapski, Molecular Hydrogen Formation (GH2) in the Radiation Chemistry of Aqueous Solutions, *J. Phys. Chem.*, 1970, **74**, 2903–2911.

99 H. A. Schwarz, Applications of the Spur Diffusion Model to the Radiation Chemistry of Aqueous Solutions, *J. Phys. Chem.*, 1969, **73**, 1928–1937.

100 S. P. Mezyk and D. M. Bartels, Temperature Dependence of Hydrogen Atom Reaction with Nitrate and Nitrite Species in Aqueous Solution, *J. Phys. Chem. A*, 1997, **101**, 6233–6237.

101 B. Smaller, E. C. Avery and J. R. Remko, EPR Pulse Radiolysis Studies of the Hydrogen Atom in Aqueous Solution. I. Reactivity of the Hydrogen Atom, *J. Chem. Phys.*, 1971, **55**, 2414–2418.

102 J. I. Savel'ev, Z. V. Ersova and M. V. Vladimirova, Radiolyse Alpha des Solutions Aqueuses d'Acide Nitrique, *Radiochimie*, 1967, **9**, 244–249.

103 N. E. Bibler, J. M. Pareizs, T. L. Fellinger and C. J. Bannochie, in *INIS-US–09-WM-07162*, Tucson, Arizona, 2007, vol. 41.

104 K. W. Bagnall, The chemistry of polonium, *Q. Rev., Chem. Soc.*, 1957, **11**, 30.
105 P. I. Artyukhin, V. I. Medvedovskii and A. D. Gel'man, Disproportionation of Pu(IV) and Pu(V) in Nitric Acid Solutions, *Zh. Neorg. Khim.*, 1959, **4**, 1324–1331.
106 H. Escure, D. Gourisse and J. Lucas, Dismutation du neptunium pentavalent en solution nitrique—I, *J. Inorg. Nucl. Chem.*, 1971, **33**, 1871–1876.
107 V. S. Koltunov and M. F. Tikhonov, Kinetics of Neptunium (5) Disproprotionation in Nitric Acid Solution, *Radiokhimiya*, 1975, **17**, 560–563.
108 Z.-M. Zhou, Y.-J. Zhang and H.-F. Du, Kinetic Studies on the Oxidation of Uranium (IV) in Nitric Acid Solution, *J. Radioanal. Nucl. Chem.*, 1994, **188**, 177–187.
109 V. S. Koltunov, V. I. Marchenko, G. I. Zhuravleva and O. A. Savilova, Kinetics of Redox Reactions of U, Pu, and Np in TBP Solutions: VII. Kinetics of Reduction of Pu(IV) and Np(VI) with Butanal Oxime in Undiluted TBP, *Radiochemistry*, 2001, **43**, 334–337.
110 C. Gregson, C. Boxall, M. Carrott, S. Edwards, M. Sarsfield, R. Taylor and D. Woodhead, Neptunium (V) Oxidation by Nitrous Acid in Nitric Acid, *Procedia Chem.*, 2012, **7**, 398–403.
111 M. Precek, PhD thesis, Oregon State University, 2013.
112 H. Chen, R. J. Taylor, M. Jobson, D. A. Woodhead, C. Boxall, A. J. Masters and S. Edwards, Simulation of Neptunium Extraction in an Advanced PUREX Process—Model Improvement, *Solvent Extr. Ion Exch.*, 2017, **35**, 1–18.
113 M. Chotkowski, Redox interactions of technetium with neptunium in acid solutions, *J. Radioanal. Nucl. Chem.*, 2018, **317**, 527–533.